Absolute emission cross section for electron-impact excitation of Li^+ to the $(2\,^3P)$ level

Wade T. Rogers, J. Østgaard Olsen,* and Gordon H. Dunn
Joint Institute for Laboratory Astrophysics, National Bureau of Standards and University of Colorado, Boulder, Colorado 80309
(Received 21 April 1978)

Crossed beams of electrons and Li^+ ions have been used to measure the absolute emission cross section for the process, $e + Li^+(1\,^1S) \rightarrow e + Li^+(n\,^3l) \rightarrow h\nu$ (548.5 nm), from below the threshold at 61.26 to 162 eV. The cross section exhibits the sharp onset at threshold characteristic of positive-ion excitation. The cross section at threshold is deduced to be 2.0×10^{-18} cm^2, decreasing to 0.2×10^{-18} cm^2 at 162 eV. Total uncertainties at a 68% confidence level are typically about $\pm 15\%$. Pronounced structure is observed in the near-threshold region. From about 1.5 times the threshold energy to the highest energies measured, the cross section follows the generally predicted E^{-3} behavior for ^1S to ^3P transitions. Theoretical predictions of the cross sections differ from one another by up to a factor of 2, and none appears to fit the data really well.

I. INTRODUCTION

To date, a limited number of cross-section measurements have been completed for electron-impact excitation of positive ions. However, there has not yet been an experimental measurement for a positive ion of an excitation which involves a change of spin. In this paper we report the measurement of the absolute total emission cross section for the process

$$e + Li^+(1\,^1S) \rightarrow e + Li^+(n^3l) \rightarrow h\nu\ 548.5\ \text{nm}. \qquad (1)$$

The process is dominated by excitation of the $2\,^3P$ level from which the 548-nm radiation originates, but may include substantial contributions from excitation of levels such as $3\,^3D$ and $3\,^3S$ which cascade to the $2\,^3P$ level. This process is a prototype for excitations involving change of spin, and hence provides a valuable reference point for theoretical calculations of such processes. In particular, the role of exchange as opposed to direct scattering can be illuminated due to the dominance of the exchange channel for spin-forbidden excitations.[1]

The type of process explored here is also of interest in high-temperature plasma diagnostics. The helium isoelectronic sequence is frequently used as an electron density diagnostic in astrophysical and laboratory plasmas.[2-7] Although the low cosmic abundance of Li precludes its direct use as an astrophysical tool, laboratory measurements on Li^+ will allow determination of the reliability of the theories for the more highly charged heliumlike ions. This determination has heretofore been impossible in a quantitative sense.

II. EXPERIMENTAL PROCEDURE

The experiment consists of bombarding target Li^+ ions with variable-energy electrons and measuring a known fraction of the 548.5-nm photons produced from the resulting excitation of the $2\,^3P$ level which radiatively decays to the $2\,^3S$ level. An energy-level diagram for Li^+ is shown in Fig. 1. The crossed-charged-beams apparatus used for this work is shown schematically in Fig. 2 and has been described in considerable detail previously.[8-10] We will discuss some general aspects of the method, but try to limit discussions of detail to those aspects which are unique to the present experiment.

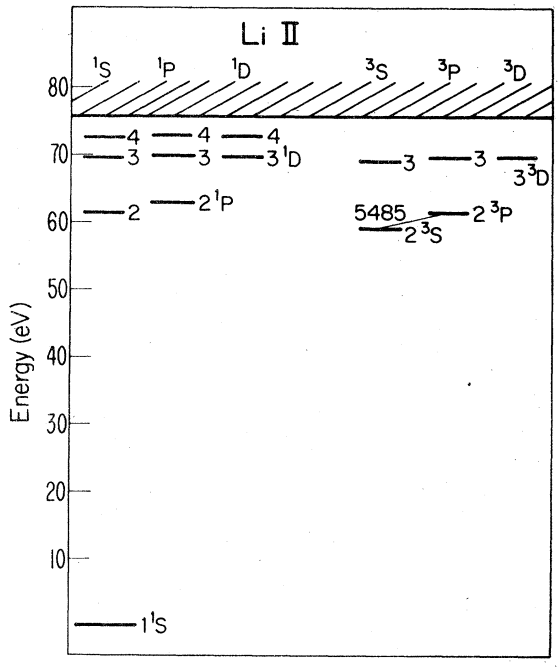

FIG. 1. Energy levels of Li II.

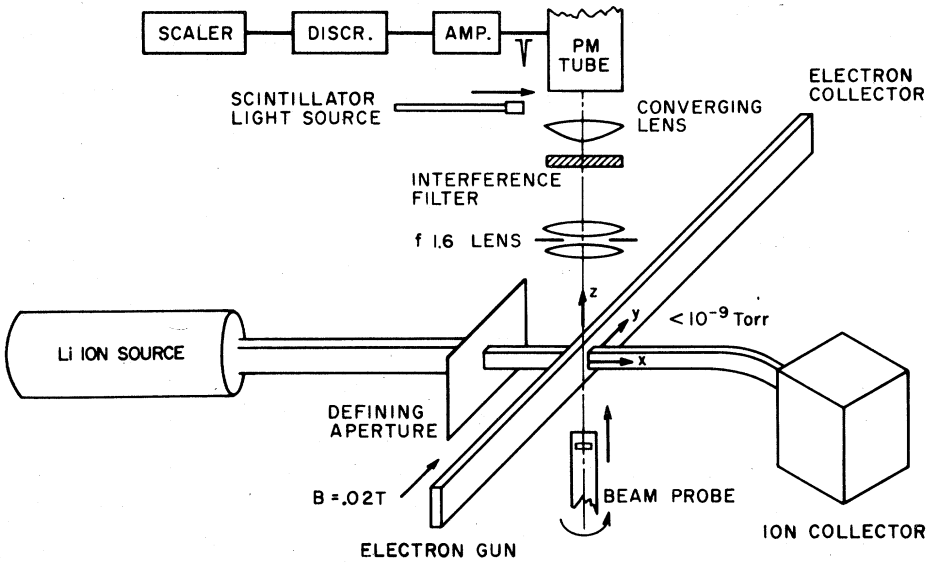

FIG. 2. Experimental arrangement.

A. Derivation of cross section from measured quantities

The cross section is obtained from measured quantities from the equation

$$\sigma = \frac{1}{Y_\Omega}\frac{\mathcal{R}}{I_i I_e}\frac{e^2 v_i v_e}{(v_i^2+v_e^2)^{1/2}}\frac{\mathcal{F}}{D(z_0,\lambda)}\,. \tag{2}$$

Here σ is the emission cross section, $\mathcal{R}$ is the photon count rate, e is the electronic charge, I_i and I_e are the total currents of ions and electrons, and v_i and v_e are the respective velocities. The factor Y_Ω corrects for anisotropy of the radiation and takes into account the finite detector solid angle Ω. It is given in terms of θ, the angle between the photon trajectory and electron beam axis, by

$$Y_\Omega = (1 - P\langle\cos^2\theta\rangle_\Omega)/(1-\tfrac{1}{3}P)\,, \tag{3}$$

where P is the polarization of photons emitted along the detection axis, and $\langle\cos^2\theta\rangle_\Omega$ is the average value of $\cos^2\theta$ over the detector solid angle. The form factor $\mathcal{F}$ accounts for the spatial overlap of the beams and the spatial variation of detector sensitivity. Let axes x, y, and z be, respectively, the directions of the ion beam, electron beam, and the axis of observation of photons. Also, let $R(z)$ and $G(z)$ represent ion- and electron-beam density distributions along the z axis and $\eta(z,\lambda)$ the relative detector sensitivity profile. The form factor is then given by

$$\mathcal{F} = \frac{\int R(z)\,dz \int G(z)\,dz}{\int R(z)G(z)\eta(z,\lambda)\,dz}\,, \tag{4}$$

where

$$\eta(z,\lambda) = D_R(z,\lambda) - I_1 + (e^{w_e/v_i\tau} - 1)I_2 \tag{5}$$

with

$$I_1 = \frac{\int_0^{w_e} e^{-x/v_i\tau} D_R(x,z,\lambda)\,dx}{\int_0^{w_e} D_R(x,z_0,\lambda)\,dx} \tag{6}$$

and

$$I_2 = \frac{\int_{w_e}^{\infty} e^{-x/v_i\tau} D_R(x,z,\lambda)\,dx}{\int_0^{w_e} D_R(x,z_0,\lambda)\,dx}\,. \tag{7}$$

The quantity $D(z_0,\lambda)$ in Eq. (2) is the average probability that a photon emitted in an arbitrary direction from the $z = z_0$ plane in the collision volume will be counted, and $D_R(z,\lambda)$ in Eq. (5) is the relative variation of that probability with height z, normalized such that $D_R(z_0,\lambda) = 1$. $D_R(x,z,\lambda)$ is the relative probability averaged over the width of the ion beam that a photon emitted from a line parallel to the electron beam will be detected, w_e is the width of the electron beam, and τ is the lifetime of the transition yielding photons of wavelength λ. In Eq. (5) the subtraction of I_1 accounts for the fact that, due to their finite lifetime, some ions do not radiate while within the electron beam, while the term including I_2 accounts for emission beyond the electron beam which is still detected. In this experiment, about 65% of the excited ions radiated beyond the field of view of the detector. This point is discussed in detail in the Appendix. As previously noted, the methods of measurement of quantities in Eqs. (2)–(7) have been discussed thoroughly elsewhere.[8,9]

B. Ion beam, electron beam, and photon detector

Ions are thermionically emitted from an indirectly heated molybdenum surface coated with β-eucryptite,[11,12] accelerated, and focused into a beam. The gun is fabricated from gold-plated OFHC copper, and the cylindrical elements are

clamped onto parallel ceramic rods. The emitter is a molybdenum cylinder, closed on one end and coated on that end with a layer approximately 0.5 mm thick of the Li-containing material, β-eucryptite. A commercial cathode heater operated at about 15 W is inserted into the open end for indirect heating of the emitter. The coating is applied in the form of a powder suspended in methanol, and then melted into a glasslike state in a hydrogen-induction furnace.

In initial tests of the source it was found by mass spectrometry that after approximately 5 h of operation, species purity of the beam was better than 99.9%; hence no mass analysis was employed. The normal isotope ratio $^7Li/^6Li = 12.5$ was also observed. Ions are extracted from the surface of the emitter by a standard Soa lens, then focused and steered by voltages on the remaining elements. The beam is transported through a differential pumping tube from the separately pumped ion-gun chamber into the interaction chamber where the pressure is typically less than 1.3×10^{-7} Pa (10^{-9} Torr). It is then refocused into a parallel beam by a three-aperture einzel lens. Final positioning of the beam is accomplished by horizontal and vertical electrostatic deflectors immediately before the collision box, and the beam is finally trapped in a collector which has been described previously.[8] By observing the beam current into the collector as a function of emission current (varied by changing heater power) we concluded that the ion beam was space-charge limited to about 6 μA at 1-keV beam energy. The life of the ion source was approximately 100 h, during which time the beam current decayed from its space-charge-limited value to about 2 μA. As ion emission decreased, the heater was turned up to maintain useable currents, and the life of the source was always terminated by heater burnout.

The electron gun used in this work is identical to the one previously described[8-10] except that some slits are changed to reduce noise originating from photons produced by electrons striking slits. As both beams were modulated and signals recorded in suitably gated dual scalers such "slit noise" would normally not have been a major problem. However, the ion beam was of high enough density that the space-charge potential of the ion beam introduced a perturbation of electron trajectories. Since the slit noise was a function of electron trajectories it turned out that there was a component of noise that was synchronously modulated in such a way as to give a "negative signal" larger in magnitude than the true signal, leading to erroneous results. The situation was resolved by reducing the electron-beam size via an upstream limiting aperture (6.35×2.0 mm), and enlarging downstream aperatures to reduce the number of electrons impinging on slits visible to the detection optics. A variety of diagnostics including tests of the cross section versus ion-beam current verified that the space-charge-modulated component of noise was eliminated.

In addition to altering the electron trajectories, the ion space charge tends to accelerate the electrons as they approach the ion beam. In order to measure this effect we measured the excitation function for the process

$$e + H_2 \rightarrow e + H(1s) + H(n = 3) \tag{8}$$

which has a threshold at 16.6 eV. The measurement was done at a variety of electron-beam currents and both with and without the ion beam traversing the collision volume. Modifying the energy calibration formula used by Taylor and Dunn[8] to account for the ion space-charge acceleration, we obtain

$$eV_e = e[V_c - \phi - (S_e/V_e^{1/2})I_e + (S_i A_i^{1/2}/V_i^{1/2})I_i], \tag{9}$$

where V_c is the cathode potential in volts, eV_e is the electron energy in electron volts, ϕ is the cathode contact potential, I_e and I_i are the electron and ion dc currents in microamperes, V_i is the ion acceleration voltage, A_i is the ion atomic weight, and S_e and S_i are geometrical constants. By measuring the H_2 and $Li^+(2\,^3P)$ thresholds we determined the constants in Eq. (9) to be $\phi = 2.1$ V, $S_e = 0.071(\pm 10\%)$ $V^{3/2}\,\mu A^{-1}$, and $S_i = 3.0(\pm 10\%)$ $V^{3/2}\,\mu A^{-1}$. Thus, for example, with a 1-keV, 6-μA beam of Li^+ there is approximately a 1.5-V ion space-charge acceleration effect; and with a 60-eV, 300-μA beam of electrons there is a 2.7-V retardation.

The photon detection system is similar to that described previously[8,9] except that all optical elements are made of high-quality ultraviolet grade quartz instead of glass. The collection lens has an $f/1.6$ aperture, producing a nominally parallel beam that passes through the vacuum window and then the interference filter before being focused about 1 cm behind the multiplier photocathode by the converging lens. The filter is tilted about 3° such that the wave length at the transmission peak is 548.8 nm, the band width is 1.9-nm full width at half maximum (FWHM), and the transmission at 548.5 nm is 51%. The dark count of the photomultiplier is typically 1.5 counts per sec when cooled to approximately −25 °C. The entire photon detection system is absolutely calibrated by the technique described previously[8,9] giving an absolute sensitivity of $D(z_0, 548.5\text{ nm}) = 1.97 \times 10^{-4}$ counts per photon with a total uncertainty of 4.5% evalu-

ated to be approximately at the 68% confidence level (68% CL), though this figure includes systematic uncertainties (see below) for which "confidence level" is ill-defined.

C. Data acquisition and reduction

As mentioned in Sec. II B a modulation scheme is employed to separate electron-ion impact signals from various background photon signals. The scheme employed[13-16] is similar to that described by Dance *et al.*[13] Normal signals encountered during cross-section measurements ranged from 0.06 to 0.8 $\sec^{-1}$, and the background was typically about 8–12 $\sec^{-1}$. Integrations of beam currents and photon signals were performed in units of 10^3 sec, with typically 70 or 80 units per data point. However, some data points required as much as 300×10^3 sec of integration, or approximately 80 h, to achieve the desired statistical precision.

Data are reduced in a straightforward way using Eq. (2) to obtain the cross section from measured quantities. Only two comments need be made here. First, the calculation of the form factor $\mathfrak{F}$ in Eqs. (2) and (4) from measured beam intensity profiles $R(z)$ and $G(z)$ is complicated by the finite lifetime correction as discussed in Sec. II D and in detail in the Appendix. Second, the anisotropy correction factor Y_Ω in Eqs. (2) and (3) requires knowledge of the polarization P. Our crossed-beams facility has the capability of measuring polarization; but, due to the extremely small signal levels, the time required to obtain even poor statistical precision was prohibitive. An estimate of the upper and lower limits of the polarization can be obtained from the work of Macek and Jaecks.[17] Taking into account the different nuclear spins of the two Li isotopes ($I=\frac{3}{2}$ for ^{7}Li, and $I=1$ for ^{6}Li) and the proper isotope ratio, but neglecting mixing between fine- and hyperfine levels,[18,19] we obtain the values $P_{\max}=11.1\%$ and $P_{\min}=-5.8\%$. Here $P_{\max}$ corresponds to $\sigma_{\pm1}/\sigma_0=0$ and $P_{\min}$ corresponds to $\sigma_0/\sigma_{\pm1}=0$, where $\sigma_{M_L}(M_L=0,\pm1)$ are the partial cross sections for excitation of the magnetic sublevels of the $2\,^3P$ state. The above values of the polarization lead to anisotropy factors Y_Ω of 1.037 and 0.982, respectively. The polarization is expected to be positive close to the excitation threshold and to asymptotically approach its minimum value at high energies. However, since we do not know in detail how the polarization varies with energy, no anisotropy correction has been applied to the data. Instead an uncertainty in Y_Ω has been allowed for by setting $Y_\Omega=1.0(^{+0.037}_{-0.018})$.

D. Uncertainties

All statistical uncertainties are quoted at the 68% confidence level (68% CL), corresponding to one standard deviation of the mean. Where systematic uncertainties of a nonstatistical nature occur, an effort has been made to assess these uncertainties at a confidence level consistent with the statistical 68% CL. Where different uncertainties are judged to be uncorrelated they are combined in quadrature to give a total uncertainty. Tables I and II list the sources of uncertainty and their quadrature combinations. Form factor and ion-velocity uncertainties are correlated through the finite lifetime correction; hence they are combined linearly before being combined in quadrature with other uncertainties. The total uncertainty is obtained for each data point in Table III by quadrature combination of the counting statistical uncertainty, relative uncertainty, and absolute uncertainty.

Not included in Tables I and II is an uncertainty in calculating $\eta(z,\lambda)$ in Eq. (5) [and thus σ in Eq. (2)] resulting from an uncertainty in the $2\,^3P$ state lifetime. We have used the theoretical lifetime of 43.94 nsec in reducing the data. There are a number of extensive calculations[20-22] including one of upper and lower bounds[22] that lead us to use this. However, there have also been a number of experimental values determined, and the beam-gas-laser experiment of Harde,[23] giving a lifetime of 37.1 nsec, seems to be that most free of difficulties. Should this experimental value prove to be correct, one would need to multiply the cross sections presented here by 0.87. This lifetime correction is discussed in greater detail in the Appendix.

III. RESULTS AND DISCUSSION

Results of the cross-section measurements appear in Table III and in Figs. 3 and 4. Error bars in the figures include only those uncertainties that may vary with energy, which we call relative uncertainties. It is noted, however, that inclusion of absolute uncertainties (i.e., those that shift the curve as a whole) makes very little visual difference in the error bars. It is noted that the maximum value of the cross section is only 2.1×10^{-18} cm^2 at about 70 eV. Data taken below the 61.26-eV threshold are zero within two standard deviations, another indication that there are no spurious intermodulation effects between the beams leading to an erroneous signal. Tests were also carried out to insure that the measured cross sections were independent of electron- and ion-beam currents, beam chopping frequency, scalar duty cycle, background gas pressure, and ion-beam energy. The rise of the signal across the threshold is consistent with an infinitely sharp onset characteristic of electron excitation of positive ions folded with

TABLE I. Experimental uncertainties.

Source of uncertainty	Percentage uncertainty
Counting statistics	
Systematic uncertainties [a]	
Form factor	1.8
Ion velocity	0.3
	2.1
Anistropy correction factor	+1.8
	−3.7
Path length of electrons	0.2
Uncollected electron current	0.5
Scintillator use	1.7
Horizontal ion beam position	2.0
Filter temperature	1.0
Electron current measurement	0.3
Ion current measurement	0.3
Total Quadrature Sum of Systematic Uncertainties	+4.0
	−5.1

[a] An attempt was made to evaluate the systematic uncertainties at a level comparable to the 68% confidence level (1 SD) at which statistical uncertainties are cited.

the 1.0-eV energy distribution of the electron beam. The near-threshold data show some structure, but from about 86 eV up to the highest energies measured the cross section is in good agreement with the E^{-3} dependence predicted for a $^1S \rightarrow {}^3P$ excitation.[24]

The structure in the near-threshold cross section is probably due at least in part to resonances of the $e + \mathrm{Li}^+$ system with doubly excited states of Li I, leading to interference effects in the excitation cross section. Such effects have been previously observed in excitation of ion resonance transitions,[8,15,25] most notably in Ba^+ and Hg^+. In Fig. 3 the locations of the $3\,^3S$ and $3\,^3D$ levels, and the ionization limit of Li II have been included for reference. It is noted that the pronounced structures below 68.8 eV should probably be associated with such resonances since they are located more than the energy spread of the electron beam below the threshold for the $3\,^3S$ level. Structures occurring at higher energies such as the one near 69 eV may well be associated with excitation of cascading ^3S and ^3D levels. Distorted wave calculations of Mann[26] for excitation of the $3\,^3S$ and $3\,^3D$ levels indicate that cascade from these levels will sum to about a 10% contribution to the total cross section between 70 and 200 eV.

Due to the pronounced structure it is questionable to deduce a threshold value of the cross section. However, by using a power-law least-squares fitting to the first three and first five points above threshold, after correcting for electron-energy spread and extrapolating back to threshold, we find $\sigma_{th} = 2.09$ and 1.86×10^{-18} cm^2, respectively. Thus, we take the threshold cross section to be $2.0 \pm 0.3 \times 10^{-18}$ cm^2.

TABLE II. Radiometric calibration uncertainties.

Source of uncertainty	Percentage uncertainty [a]
Projected source area A_Ω	0.3
Calculated strip lamp radiance	2.0
Response to strip lamp	1.1
Transfer factor	3.7
Radiometric integrals	1.0
Total Quadrature Sum	4.5

[a] An attempt was made to evaluate the systematic uncertainties at a level comparable to the 68% confidence level (1 SD) at which statistical uncertainties are cited.

TABLE III. Measured emission cross sections for electron-impact excitation of Li^+ ($1\,^1S$) to give 548-nm line from Li^+ ($2\,^3P$) → Li^+ ($2\,^3S$).

Energy (eV)	Cross section (10^{-19} cm^2)	Total uncertainty[a] (10^{-19} cm^2)
52.7	4.7	3.8
55.9	−3.0	1.4
57.4	0.25	1.1
60.8	2.8	1.0
61.8	17.9	1.3
62.4	15.6	1.9
63.3	14.3	1.5
64.9	14.5	1.5
65.5	12.7	1.1
66.5	17.6	1.4
67.8	17.3	1.5
69.2	20.0	1.7
69.7	21.2	4.2
71.2	15.6	1.1
73.9	15.8	1.2
75.4	13.9	1.3
77.1	16.7	2.0
77.6	16.1	3.2
85.8	13.0	1.8
97.2	8.4	0.8
97.8	9.2	2.3
115.6	7.5	0.6
130.9	4.7	0.8
161.5	1.9	0.4

[a] Total is a combination (see text) of statistical and systematic uncertainties taken at what is estimated to be equivalent to the 68% confidence level (one standard deviation).

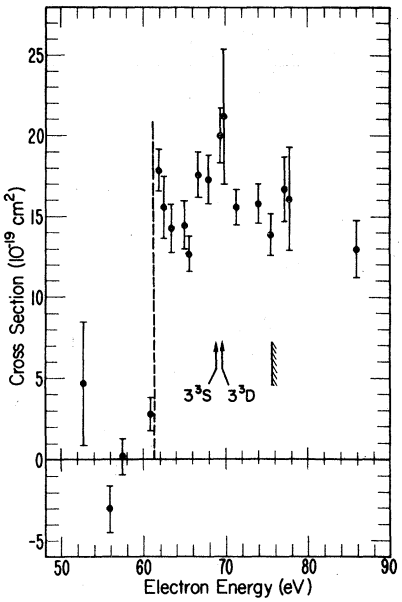

FIG. 3. Measured cross section vs electron energy for emission of 548.5-nm line from bombardment of Li^+ ($1\,^1S$). Uncertainties include statistical and only those systematic uncertainties which may vary with energy and thus change the shape of the curve (these dominate total uncertainty).

Figure 4 includes several theoretical calculations for comparison. Each of the calculations is presented only for excitation of the $2\,^3P$ level, whereas the experimental results may include cascade contributions discussed above.[26] The theoretical pre-

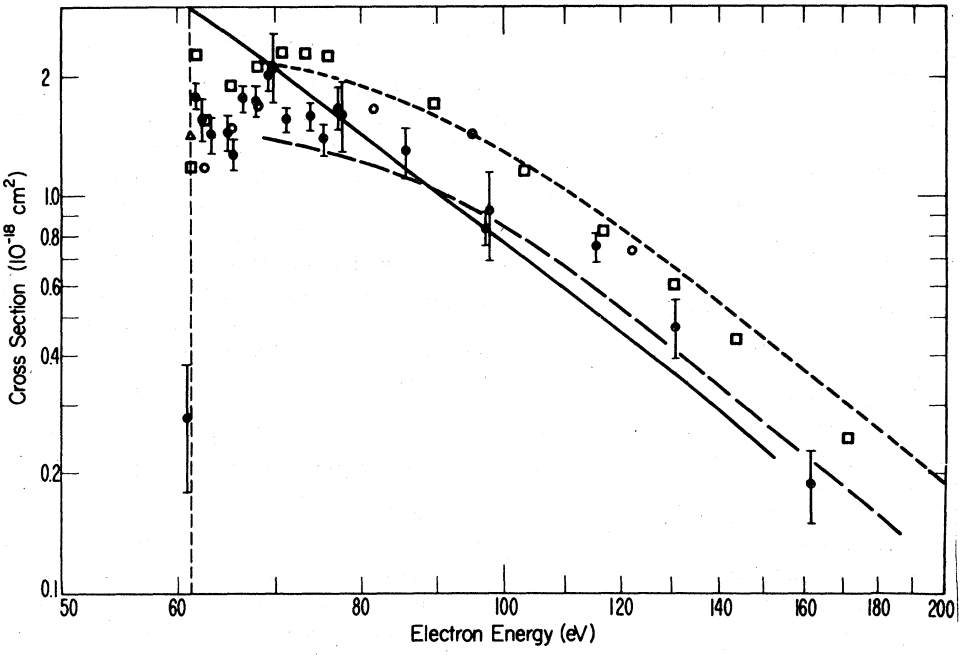

FIG. 4. Log-log plot of cross section vs electron energy for excitation of the $2\,^3P$ level of Li^+ from bombarding Li^+ ($1\,^1S$). Present experiment for emission of 548.5-nm radiation, ‡; DW, Norcross and Hummer (Ref. 27), long dashes; DW, Bhatia and Temkin (Ref. 28), short dashes; CPCO, Tully (Ref. 29), solid curve; method of orthogonalized functions, Vainshtein (Ref. 1), △; 5CC, Robb (Ref. 32), □; 5CC, Cooper (Ref. 33), ○. Uncertainties include statistical and only those systematic uncertainties which may vary with energy and thus change the shape of the curve (these dominate total uncertainty).

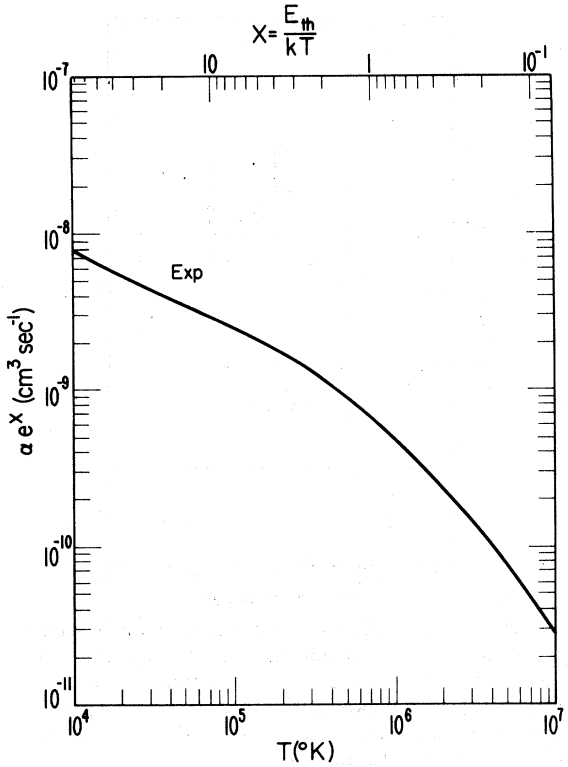

FIG. 5. Rate coefficient α times e^X ($X=E_{th}/kT$) vs temperature for emission of 548.5-nm Li^+ line due to bombardment of Li^+ ($1\,^1S$). Values assume a Maxwellian electron velocity distribution and are computed according to Ref. 35.

dictions differ from one another by up to a factor of 2, and none fits the data really well. The long- and short-dashed curves in Fig. 4 show distorted wave (DW) calculations of Norcross and Hummer[27] and of Bhatia and Temkin,[28] respectively. Mann[26] has also done a number of DW and Coulomb-Born (CB) calculations, producing a number of intersecting curves between his high DW curve and Hummer and Norcross' curve. The solid curve is from Tully[29] who calls his approximation the Coulomb-projected Coulomb-Oppenheimer (CPCO) approximation, which is a modification of the exchange approximation of Oppenheimer[30] and is closely related to the Coulomb-projected Born approximation of Geltman.[31] Tully's result is essentially a pure E^{-3} cross section from threshold, and at threshold his cross section is larger than experiment by a factor of ~1.5. Vainshtein[1] reports only a threshold value for the $Li^*(2\,^3P)$ excitation cross section, which is smaller than experiment by a factor of 1.4. The open squares show five-state close-coupling calculations of Robb,[32] where he has used configuration-interaction wave functions leading to a threshold energy of 61.136 eV. His three low-energy points distinctly show a resonance below the $2\,^1P$ threshold—consistent with the experimental data. The open circles are five-state close-coupling (5CC) calculations of Cooper[33] using wave functions generated in a way described by Burke *et al.*[34]

Rate coefficients α calculated[35] from a fit to the data are shown in Fig. 5 plotted as αe^x where $x=E_{th}/kT$ and E_{th} is threshold energy. Because of the infinite rise of cross sections at threshold for ions, the threshold value and near threshold resonances of cross sections are of paramount importance in determining rate coefficients for temperatures corresponding to $kT \lesssim E_{th}$. For this reason it is important to develop a theory that can accurately predict the behavior in the near-threshold region.

IV. CONCLUSIONS

We have measured the emission cross sections for electron-impact excitation of $Li^*(1\,^1S)$ to give 548.5-nm radiation from the $Li^*(2\,^3P)$ level. The cross section at threshold is $2.0\pm0.3\times10^{-18}$ cm^2. From threshold to the Li II ionization limit the cross section shows oscillatory structure, believed to be caused by resonances with doubly excited autoionizing states of Li I, enhanced by cascade effects. Above the ionization limit the cross section follows the generally predicted E^{-3} energy dependence. Theoretical predictions of the cross sections differ from one another by up to a factor of 2, and none appears to fit the data really well. The disparities near threshold of about 50% between theoretical and experimental values lead to similar differences in computed rate coefficients.

ACKNOWLEDGMENTS

We are grateful to Dr. D. W. Norcross, Dr. D. G. Hummer, Dr. W. D. Robb, Dr. J. Mann, Dr. J. W. Cooper, and Dr. J. A. Tully for communicating their theoretical results prior to publication. Thanks are also due to Dr. Roy Garstang for several helpful discussions and to Dr. W. C. Lineberger for help with the β-eucryptite technology. This work was supported in part by the Division of Magnetic Fusion Energy, U. S. Department of Energy. One of us(J.Ø.O.) wishes to acknowledge a travel grant from the Danish National Science Research Council.

APPENDIX: FINITE-LIFETIME CORRECTION

The sensitivity function $\eta(z,\lambda)$ defined in Eq. (5) contains terms that allow for the finite lifetime of the excited state, and thus account for the fact that ions radiate from a position other than where they become impact excited even beyond the field

of sensitivity of the detector. Indeed, in this experiment the high beam velocity (1.7×10^7 cm sec^{-1} at 1 keV) and long lifetime (44 nsec) have a product almost twice the length of the detection region; thus about 65% of the ions radiate beyond the detector field of view.

Due to the magnitude of the correction it must be verified that the correction is quite accurate, otherwise large uncertainties will be carried into the cross-section determination. Furthermore, there is a striking disagreement between benchmark theoretical values of the $2\,^3P$ lifetime and a clean lifetime measurement, leaving one in doubt as to which value is correct.

The quantity $D_R(x,z,\lambda)$ in Eqs. (6) and (7) is accurately measured by stepping a source of radiation at wavelength λ (consisting of a narrow slit parallel to the electron-beam direction) along the direction of ion motion x, repeating for a variety of heights z, and recording the response of the photon detection system at each position. Integrals I_1 and I_2 [Eqs. (6) and (7)] are computed numerically and combined with $D_R(z,\lambda)$ to obtain $\eta(z,\lambda)$ [Eq. (5)]. $\eta(z,\lambda)$ is then folded with beam profiles for each data point to obtain the form factor $\mathfrak{F}$ [Eq. (4)].

In order to derive a simple analytic formula for the lifetime correction let us assume that $D_R(x,z,\lambda)$ is nonzero and independent of x for $0\leq x\leq L$ and zero for $x>L$, $x=0$ being defined as the leading edge of the electron beam. For the nonzero value of $D(x,z,\lambda)$ we take its average value over the electron beam, i.e.,

$$f(z,\lambda)\equiv\begin{cases}\dfrac{1}{w_e}\displaystyle\int_0^{w_e} D(x,z,\lambda)\,dx & \text{for } 0\leq x\leq L,\\ 0 & \text{for } x>L.\end{cases} \tag{A1}$$

With this definition of $f(z,\lambda)$ we have

$$f(z,\lambda)/f(z_0,\lambda)\simeq D_R(z,\lambda). \tag{A2}$$

Using these approximations in Eqs. (5)–(7) we get

$$\eta(z,\lambda)\simeq D_R(z,\lambda)\left[1-\frac{v_i\tau}{w_e}\,e^{-L/v_i\tau}\left(e^{w_e/v_i\tau}-1\right)\right]. \tag{A3}$$

Defining the z-independent quantity T by Eq. (A3):

$$\eta(z,\lambda)=D_R(z,\lambda)(1-T) \tag{A4}$$

we can write Eq. (4) as

$$\mathfrak{F}\simeq[1/(1-T)]\mathfrak{F}_0, \tag{A5}$$

where $\mathfrak{F}_0$ is the form factor for $\tau=0$.

In order to test the validity of the above approximations both $\mathfrak{F}$ and $\mathfrak{F}_0$ were computed numerically for all beam profiles measured.[36] It was found that the standard deviation *about* the mean of 50 samples amounts to less than ±1%. Thus it is valid to a good approximation to take T as independent of z, which means that the finite lifetime correction may be factored out of Eq. (4) in the way described above.

For given values of v_i, τ, and w_e we can determine an effective observation length L so that the numerically calculated value of $\mathfrak{F}_0/\mathfrak{F}$ is reproduced using formulas (A3) and (A5). With $v_i=1.66\times10^7$ cm sec^{-1}, $w_e=0.160$ cm, and $\tau=43.94\times10^{-9}$ sec (see below), we obtain $L=0.386$ cm.

Additional checks of the lifetime correction formula have been performed by calculating from Eqs. (A3) and (A5) the ratio $\mathfrak{F}_0/\mathfrak{F}$ for a number of different values of v_i and τ, deviating as much as 50% from the value above. In all cases the $\mathfrak{F}_0/\mathfrak{F}$ value obtained in this way agreed to within 1% with the corresponding value obtained by numerical integration of Eqs. (4)–(7).

The uncertainty in the form factor (4) can be estimated from Eq. (A3). By estimating the errors associated with the measurement of $D(x,z,\lambda)$ and with the determination of the electron beam width w_e,[36] one can use Eq. (A3) to compute the associated error in $1-T$ to be about 0.9%. This uncertainty is included in quadrature with the 1.5% form factor uncertainty due to beam profile measurement in Table I to obtain a total form factor uncertainty of 1.8%.

Table IV summarizes the present state of knowledge of the lifetime of $Li^+(2\,^3P)$. There is excellent agreement among the various theoretical calculations. The upper and lower bounds of Anderson and Weinhold[22] represent absolute uncertainties beyond which exact non relativistic quantum theory could never fall, and nicely bracket the result of Schiff *et al.*[21] The experimental situation is not so well resolved. Of the four experiments quoted the beam-gas-laser experiment by Harde[23] seems to be by far the cleanest experiment, being presumably free of cascade effects, yet the disagreement with the very sophisticated theories is disturbing. Although we see no reason to doubt the accuracy of this experiment, we are nevertheless compelled to believe the validity of the theory, since it is almost inconceivable that it could be wrong beyond the 1% level. Therefore, we have chosen to use $\tau=43.94$ nsec to reduce our data. Should it be shown in the future that the theory is incorrect, our results can be corrected using (A4) and (A6), taking $L=0.386$ cm, $v_i=1.66\times10^7$ cm sec^{-1}, and $w_e=0.160$ cm. The cross section is then corrected according to

$$\sigma_c=\sigma_p\,[0.341/(1-T_c)], \tag{A6}$$

where σ_p is the cross section reported here, and

TABLE IV. Lifetime values of Li^+ ($2\,^3P$).

τ (nsec)	Method	Ref. (year)
	Theory	
43.9	central-field approximation	Ref. 20 (1965)
43.94	220-term series solution to Schrödinger equation	Ref. 21 (1971)
43.97ub 43.92lb	variational absolute upper, lower bounds	Ref. 22 (1974)
	Experiment	
54.4 ± 2.7	beam-gas	Ref. 37 (1967)
32 ± 2	beam-foil	Ref. 38 (1969)
45 ± 5	rf magnetic resonance	Ref. 39 (1973)
37.1 ± 0.4	beam-gas-laser	Ref. 23 (1975)

σ_c and T_c are the corrected cross section and lifetime correction, respectively. The 37.1-nsec lifetime of Harde would give $\sigma_c = 0.87\sigma_p$.

It is noted that the lifetimes of the cascading $3\,^3S$ and $3\,^3D$ levels are 3.5 and 0.9 nsec, respectively, and viewing of cascading levels will be limited only by the 44-nsec lifetime of the $2\,^3P$ level, i.e., the same lifetime corrections will apply.

*On leave of absence from the Institute of Physics, University of Aarhus, DK-8000 Aarhus C, Denmark.
†Staff Member, Quantum Physics Division, National Bureau of Standards.

[1]L. A. Vainshtein, Zh. Teor. Eksp. Fiz. 67, 63 (1974). [Sov. Phys. JETP 40, 32 (1975)].
[2]A. H. Gabriel and C. Jordan, *Case Studies in Atomic Collision Physics II*, edited by E. W. McDaniel and M. R. C. McDowell (North-Holland, Amsterdam, 1972), pp. 211–294.
[3]A. H. Gabriel and C. Jordan, Mon. Not. R. Astron. Soc. 145, 241 (1969).
[4]H.-J. Kunze, A. H. Gabriel, and H. R. Griem, Phys. Rev. 165, 267 (1968).
[5]O. Bely, Phys. Lett. A 26, 408 (1968).
[6]A. Burgess, D. G. Hummer, and J. A. Tully, Philos. Trans. R. Astron. Soc. Lond. 266, 225 (1970).
[7]W. Englehardt, W. Köppendörfer, and J. Sommer, Phys. Rev. A 6, 1908 (1972).
[8]P. O. Taylor and G. H. Dunn, Phys. Rev. A 8, 2304 (1973).
[9]P. O. Taylor, Ph.D. thesis (University of Colorado, 1972) (unpublished). Available through University Microfilms, Inc., Ann Arbor, Mich.
[10]P. O. Taylor, K. T. Dolder, W. E. Kauppila, and G. H. Dunn, Rev. Sci. Instrum. 45, 538 (1974).
[11]S. K. Allison and M. Kamegai, Rev. Sci. Instrum. 32, 1090 (1961).
[12]R. K. Feeney, W. E. Sayle, II, and J. W. Hooper, Rev. Sci. Instrum. 47, 964 (1976).
[13]D. F. Dance, M. F. A. Harrison, and A. C. H. Smith, Proc. R. Soc. Lond. A 290, 74 (1966).
[14]Circuitry for the more sophisticated beam-modulation scheme was developed after it was discovered that the previously used scheme (Ref. 8) was inadequate to reliably separate signal from background at less than the 1 in 10^3 level which was encountered in the measurement of very small cross sections here and in Ref. 15. The scheme employs a 2-MHz (or other) clock with countdown logic circuits to develop the pulse trains for modulating the electron and ion beams and for gating the two scalers. Included in the scheme are refinements (Ref. 16) for averaging any irregularities across the current pulses or between scalers, and other refinements for shortening the scaler duty cycle to avoid counting during beam switching transients. The signal is obtained by subtracting the counts registered by the two scalers after sufficient time has elapsed to produce the desired statistical precision, and the signal can be separated from a background 10^4 larger.
[15]D. H. Crandall, R. A. Phaneuf, and G. H. Dunn, Phys. Rev. A 11, 1223 (1975).
[16]L. Molyneux, K. T. Dolder, and B. Peart, J. Phys. E 4, 149 (1971).
[17]J. Macek and D. H. Jaecks, Phys. Rev. A 4, 2288 (1971).
[18]H. G. Berry, J. L. Subtil, E. H. Pinnington, H. J. Andrä, W. Wittmann, and A. Gaupp, Phys. Rev. A 7, 1609 (1973).
[19]H. G. Berry, E. H. Pinnington, and J. L. Subtil, Phys. Rev. A 10, 1065 (1974).
[20]W. L. Wiese, M. W. Smith, and B. M. Glennon, *Atomic Transition Probabilities, Vol. I* (NSRDS-NBS 4, 1966), p. 19. [Data are cited from A. W. Weiss (private communication).]

[21]B. Schiff, C. L. Pekeris, and Y. Accad, Phys. Rev. A 4, 885 (1971).
[22]M. T. Anderson and F. Weinhold, Phys. Rev. A 9, 118 (1974).
[23]H. Harde, in *Proceedings of the Fourth International Conference on Beam-Foil Spectroscopy*, edited by I. Sellin and D. Pegg (Plenum, New York, 1975), p. 859.
[24]I. I. Sobelman, *An Introduction to the Theory of Atomic Spectra* (Pergamon, New York, 1972), p. 518.
[25]D. H. Crandall, P. O. Taylor, and G. H. Dunn, Phys. Rev. A 10, 141 (1974).
[26]J. Mann (private communication from W. D. Robb).
[27]D. W. Norcross and D. G. Hummer (private communication).
[28]A. K. Bhatia and A. Temkin, J. Phys. B 10, 2893 (1977).
[29]J. A. Tully (private communication).
[30]J. R. Oppenheimer, Phys. Rev. 32, 361 (1928).
[31]S. Geltman, Phys. Rev. 102, 171 (1956); see also J. Phys. B 4, 1288 (1971).
[32]W. D. Robb (private communication).
[33]J. W. Cooper (private communication).
[34]P. G. Burke, J. W. Cooper, and S. Ormonde, Phys. Rev. 183, 245 (1969).
[35]D. H. Crandall, G. H. Dunn, A. Gallagher, D. G. Hummer, C. V. Kunasz, D. Leep, and P. O. Taylor, Astrophys. J. 191, 789 (1974).
[36]In the numerical form factor calculations the electron-beam width was taken to be the width of the electron-beam-limiting aperture, $w_e = 0.20$ cm. However, since the confining magnetic field is stronger at the collision volume than at the aperture (Ref. 10), the actual electron-beam cross-sectional area of the collision volume is smaller than the aperture. With the present experimental setup it is not possible to measure the beam width. It was therefore assumed that the relative reduction in beam width is equal to the relative reduction in beam height. From the measured vertical electron-beam profiles and the known height of the limiting aperture (6.35 mm) it was found that this reduction amounts to $20.0 \pm 2.0\%$ which gives an effective beam width of 1.60 ± 0.04 mm. Since $\mathfrak{F}_0$, the form factor corresponding to $\tau = 0$, is independent of w_e, the form factors $\mathfrak{F}$ can be corrected for the effect of the reduced beam width using Eqs. (A3) and (A5) with the values $v_i = 1.6 \times 10^7$ cm sec^{-1}, $\tau = 43.94 \times 10^{-9}$ sec, and $L = 0.386$ cm. This correction of the form factors and thereby the cross sections is 5.9%.
[37]J. P. Buchet, A. Denis, J. Desesquelles, and M. Dufay, C. R. Acad. Sci. B 265, 471 (1967).
[38]W. S. Bickel, I. Martinson, L. Lundin, R. Buchta, J. Bromander, and I. Bergström, J. Opt. Soc. Am. 59, 830 (1969).
[39]A. Adler, W. Kahan, R. Novick, and T. Lucatorto, Phys. Rev. A 7, 967 (1973).